Aeroelastic Stability of the LCTR2 Civil Tiltrotor

C. W. Acree, Jr.
Cecil.W.Acree@nasa.gov

Wayne Johnson
Wayne.Johnson@nasa.gov

NASA Ames Research Center, Moffett Field, California 94035, USA

Abstract

A new generation of very large tiltrotors is being studied to meet emerging transportation requirements. With gross weights well in excess of 100,000 lb, such aircraft will require new technologies for acceptable weight. Wings and rotors will have different per-rev frequencies and mode shapes than current tiltrotors, so coupling between destabilizing aeroelastic modes may differ from past experience. This paper presents aeroelastic stability analyses for a Large Civil Tiltrotor (LCTR2), with emphasis on combined rotor/airframe stability (whirl flutter) in cruise. LCTR2 design features include low cruise tip speed of 400 ft/sec, a four-bladed hingeless rotor, and a structurally tapered composite wing. The effects on whirl-mode stability of wing and rotor structural properties (mass and stiffness), control-system stiffness, solidity, precone, and cruise tip speed were examined using CAMRAD II. Common nonlinear trends of damping were seen for several structural parameters for both the rotor and wing.

Notation

A	rotor disk area
c_d	section drag coefficient
c_l	section lift coefficient
$C_{L\max}$	maximum wing lift coefficient
c_m	section pitching moment coefficient
C_T	rotor thrust coefficient, $T/(\rho A V_{tip}^2)$
C_W	rotor weight coefficient, $W/(\rho A V_{tip}^2)$
D	drag
$L/D_{\max}$	maximum section lift over drag
M	Mach number
M_{dd}	drag-divergence Mach number
q	dynamic pressure
R	rotor radius
t/c	thickness to chord ratio
T	rotor thrust
V	airspeed
V_{br}	aircraft best-range speed
V_{tip}	rotor tip speed
W	gross weight
ρ	air density
σ	rotor solidity (thrust-weighted)
ISA	International Standard Atmosphere
JVX	Joint Vertical Experimental
LCTR	Large Civil Tilt Rotor
LRA	LCTR Reference Airfoils
MCP	Maximum Continuous Power
MRP	Maximum Rated Power (take-off power)
OGE	Out of Ground Effect
SFC	Specific Fuel Consumption
SLS	Sea-Level Standard conditions
SNI	Simultaneous Non-Interfering approach

Presented at the AHS Technical Specialists' Meeting, Dallas, Texas, October 15-17, 2008. *This material is declared a work of the U. S. Government and is not subject to copyright protection.*

Introduction: the LCTR Concept

The Large Civil Tiltrotor (LCTR), was developed as part of the NASA Heavy Lift Systems Investigation (Ref. 1). The concept has since evolved into the 2nd generation LCTR2 (Fig. 1), described in detail in Ref. 2. Mission specifications and key design values are summarized in Tables 1 and 2. A parallel military concept, the High Efficiency Tiltrotor (HETR) is also under study (Ref. 3).

To distinguish the different stages of the design, this paper uses LCTR to refer to the overall concept, and LCTR1 and LCTR2 to refer respectively to the design developed during the original systems investigation (Ref. 1) and the refined design described in Ref. 2 and studied herein.

This paper extends the work of Refs. 1 and 4 to a more comprehensive examination of tiltrotor aeroelastic stability, concentrating on high-speed cruise for the LCTR2. The effects on stability of wing and rotor structural properties, rotor control-system stiffness and solidity, and cruise tip speed are examined. The critical requirement is adequate whirl-flutter speed margin in cruise, because whirl flutter includes the aeroelastic effects of the airframe and the rotor. CAMRAD II (Release 4.6, Ref. 5) was used to conduct the analyses.

As a proprotor grows larger, its rotational speed must be reduce to maintain acceptable tip speed. The LCTR2 is a hingeless, slowed-rotor design, with even lower tip speeds than existing tiltrotors (V-22 and BA609). The benefits of a slowed proprotor were first demonstrated by the XV-3 (Ref. 6); a more recent variation on the concept is presented in Ref. 7. While slowing the rotor reduces the destabilizing rotor forces that drive whirl flutter, it potentially exacerbates the problem of frequency placement and modal coupling.

Wing modal frequencies do not scale with rotor speed, especially for tiltrotors designed to different mission requirements. Hingeless proprotors will have different per-rev frequencies and mode shapes than the gimbaled rotors on current tiltrotors, so coupling between wing and rotor modes may differ from past experience. Thus, there is no guarantee that current methods of specifying wing frequency placement will suffice to ensure aeroelastic stability.

These issues are the motivation for the present research. The goal is to develop criteria for inclusion in design codes to ensure that conceptual weights and geometries are consistent with aeroelastic stability. The immediate objective is to characterize the relative sensitivity of whirl-mode stability to different design parameters. The possible design matrix is extremely large, and this paper can only begin to lay out the technical explorations needed for complete understanding of the impact of aeroelastic stability on very large tiltrotors. Results are presented for traditional, basic parameter variations, with the intention of eventually incorporating the most important trends into a design code.

LCTR Design Criteria

The LCTR2 is focused on the short-haul regional market (Fig. 1). It is designed to carry 90 passengers at 300 knots over at least 1000-nm range. It has low disk loading and low tip speed of 650 ft/sec in hover and 400 ft/sec in cruise. A two-speed gearbox is assumed, so that the engine operates efficiently in both hover and cruise. This is a lower tip-speed ratio than was demonstrated in flight by the XV-3, and nearly the same gearbox speed ratio (Ref. 6). Aircraft technology projections from the LCTR1 have been updated for the LCTR2 based on a service entry date of 2018. Table 1 summarizes the nominal mission, and Table 2 lists key design values.

The following paragraphs summarize the design criteria for the LCTR2; see Ref. 2 for further details of the design process.

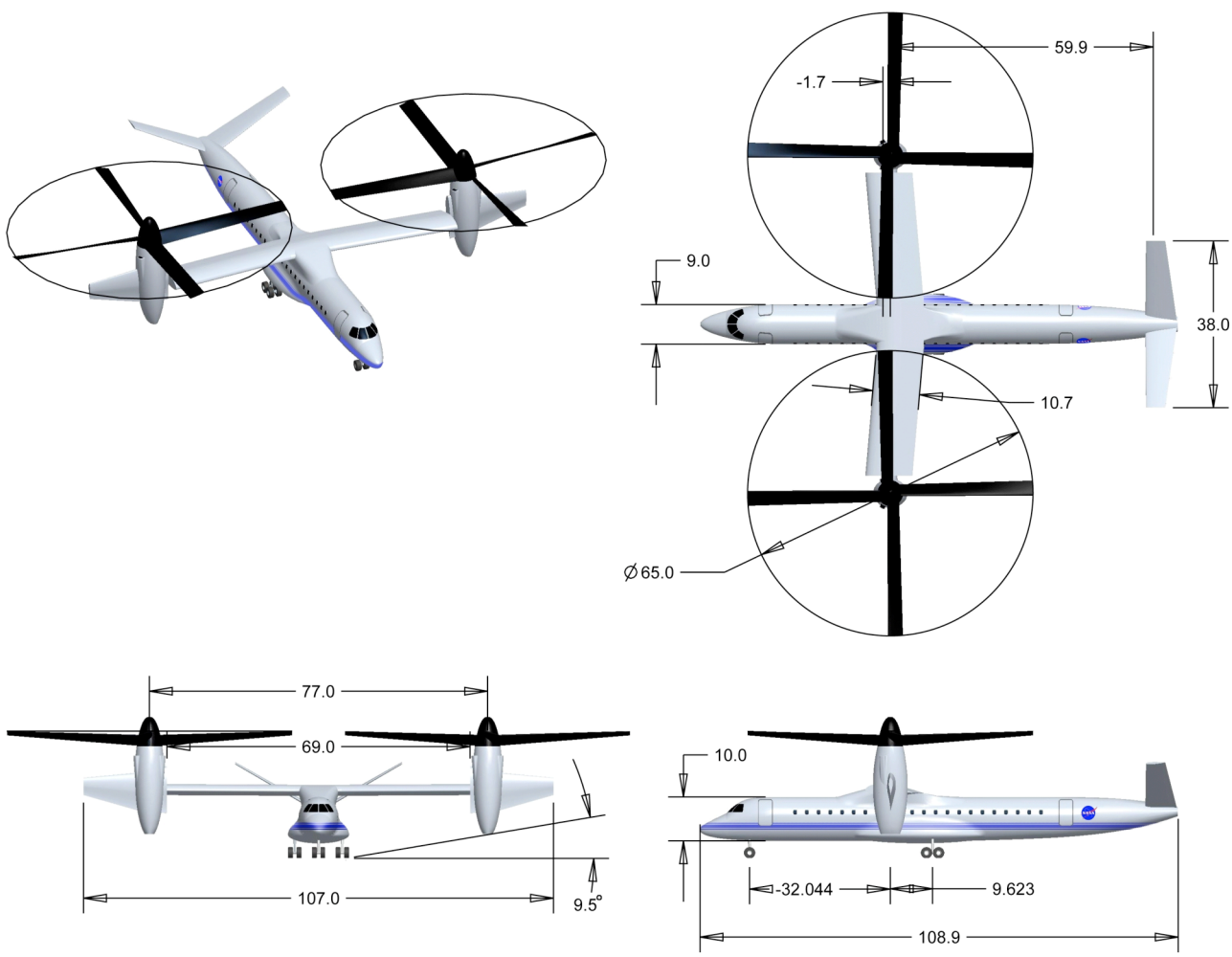

Fig. 1. The NASA Large Civil Tiltrotor, evolved version (dimensions in feet).

Table 1. LCTR2 notional mission capability.

Mission summary
Takeoff + 2 min hover OGE 5k ISA+20°C
Climb at V_{br} (credit distance to cruise segment)
Cruise at V_{br} for at least 1000 nm range, 28k ISA
Descend at V_{br} (no range credit)
1 min hover OGE + landing 5k ISA+20°C
Reserve: 30 nm + 30 min at V_{br} 28k ISA
Operational requirements
One engine inoperative: Category A at 5k ISA+20°C
All-weather operations: CAT IIIC SNI, Free Flight
45-deg banked turn at 80 knots, 5k ISA+20°C, 90% MCP

Table 2. Design values for LCTR2.

Design Constraint	Value
Payload (90 pax), lb	19,800
Cruise speed (90% MCP), knots	300
Length, ft	108.9
Wing span, ft	107.0
Wing loading, lb/ft^2	107.4
Wing sweep	−5.0 deg
Engine power, hp	4×7500
SFC (at MRP, SLS), lb/hr/hp	0.373
Rotor radius, ft	32.5
Rotor separation, ft	77.0
Number of blades	4
Precone, deg	6.0
Tip speed, hover, ft/sec	650
Tip speed, cruise, ft/sec	400
Hover C_W/σ	0.133
Baseline Design	**Result**
Gross weight, lb	107,500
Rotor weight, lb (both rotors)	8756
Wing weight, lb (zero fuel)	16,778
Fuselage empty weight, lb	14,233
Engines and drive train, lb	11,872
Cruise SFC, lb/hr/hp	0.375
Mission fuel, lb	20,408
Rotor solidity	0.130
Rotor taper (tip/root chord)	0.7
Hover C_T/σ	0.166
Cruise C_T/σ	0.0867
Disk loading, lb/ft^2	16.2
Wing area, ft^2	1001
Drag D/q, ft^2	33.9

The Design Constraint column of Table 2 includes values directly determined by the mission requirements of Table 1, such as payload, and values reflecting the level of technology assumed to be available for production, such as active controls, engine SFC, etc., based on service entry in 2018. Active loads control is assumed (but not active stability augmentation). The Baseline Design column summarizes the results of the design synthesis.

The rotorcraft design software (RC) performed the sizing of the rotorcraft. It includes mission performance analysis, generates airframe and rotor geometry, and calculates overall size, weight, and installed power. RC was developed by the Aviation Advanced Design Office of the U. S. Army Aeroflightdynamics Directorate (AFDD), RDECOM (Ref. 10).

For LCTR2, the RC design code determined the design values of Table 2 from the mission specifications of Table 1. CAMRAD II then analyzed the aerodynamics in detail, including performance in turns, rotor/wing interference, and rotor performance optimization, as described in detail in Ref. 2. CAMRAD II is an aeromechanical analysis for rotorcraft that incorporates a combination of advanced technologies, including multibody dynamics, nonlinear finite elements, and a multiple-rotor free-wake model (Ref. 5).

LCTR2 Sizing Criteria

Current trends in the marketplace point to significant future demand for aircraft seating 80 to 100 passengers. A nominal all-economy configuration of 90 passengers was accordingly established as a design criterion for LCTR2. A 32-in seat pitch and 3×2 seating layout immediately determined the payload and fuselage size in Table 2.

In the case of the LCTR2, it was recognized that to be economically feasible the engine should be a derivative design. An engine of the 7500-shp class was identified as being a viable option for LCTR2. Such an engine was assumed to include advanced technology insertion to improve power-to-weight and specific fuel consumption. A two-speed gearbox was retained, as in the LCTR1 design, to allow for operation of the derivative engine over a typical rpm range.

LCTR1 had a low-wing layout, with nontilting engines. LCTR2 returned to a more conventional high-wing, tilting engine nacelle configuration. The high wing provides better clearance for the engine exhaust when tilted upward for helicopter mode operations. The packaging of engines, transmission, and rotor shaft is more efficiently accomplished with fully tilting engine nacelles than with the fixed engine/tilting rotor configuration explored in the LCTR1 design. Additionally, the LCTR2 wing extends beyond the nacelle with tilting wing extensions, which reduce induced drag by increasing wing span in cruise. The inner wing aspect ratio is also increased as compared with LCTR1.

Design Evolution of LCTR2

Reference 2 discusses in detail performance optimization of the LCTR2 rotor. Key results of that effort were to increase rotor solidity for better turn performance and to slightly increase tip speed; wing span was also increased. Since then, further studies (Ref. 11) have suggested that adequate performance can be obtained with solidity lower than that chosen in Ref. 2 (turn performance was improved via better flap scheduling and optimization of nacelle tilt); a longer wing is not necessary.

Accordingly, the present study adopted a rotor solidity of 0.13 (the value generated by RC) and a tip speed of 400 ft/sec (the optimized value determined by CAMRAD II). The shorter wing span was also retained (Table 2).

CAMRAD II Rotor Model

The CAMRAD II rotor model of the LCTR2 had five elastic beam elements per blade, with full control-system kinematics, and 15 aerodynamic panels per blade. Blade aerodynamics were modeled as a lifting line coupled to a free-wake analysis. An isolated-rotor, axisymmetric solution was used for hover and cruise performance optimization. Blade-section aerodynamic properties were read from 2-D coefficient tables (discussed in more detail in the next section).

The CAMRAD II rotor model for LCTR2 evolved from the JVX rotor model of Refs. 12 and 13. The JVX rotor was an experimental precursor to the V-22 rotor. Its test history and relationship to the production V-22 rotor are discussed in Ref. 12.

To create the LCTR2 analytical model, the CAMRAD II model for JVX was modified to include four blades, then scaled up to LCTR2 diameter and solidity. The blade structure is an adaptation of that developed for LCTR1 (Refs. 1 and 14). The last step was to replace the JVX airfoil tables (XN-series airfoils, Ref. 15) with newly-developed tables (discussed in the next section).

The control system model included a swashplate, pitch links and pitch horns. Full kinematics are modeled, and control system flexibility was lumped into pitch-link stiffness (swashplate stiffness was set extremely high). The baseline model used rigid pitch links in order to decouple pitch-link stiffness effects on stability from rotor and wing mass and stiffness effects. This was one of the few areas where a dynamically important property could be completely isolated from other properties during stability analyses.

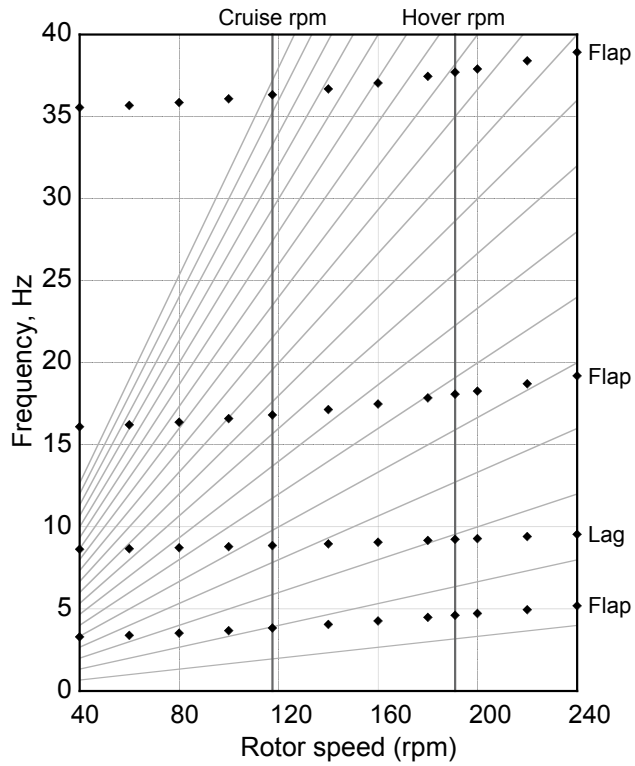

Fig. 2. Rotor frequencies at hover collective (10 deg).

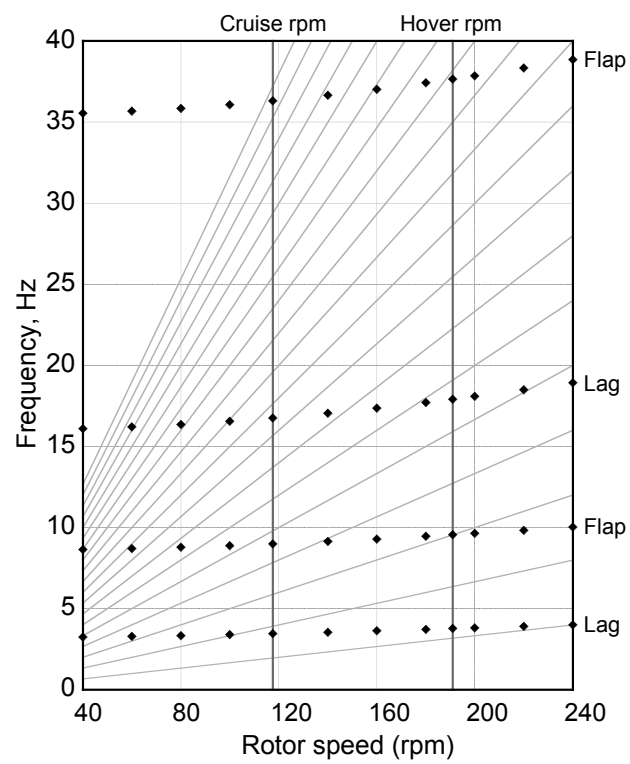

Fig. 3. Rotor frequencies at cruise collective (60 deg).

Figures 2 and 3 show the blade frequency placement at 10- and 60-deg collective, corresponding to hover and cruise conditions. Flap and lag are here defined relative to the rotor plane, so the first three modes exchange direction of dominant motion as collective varies from hover to cruise. The first flap/lag mode lies between 1/rev and 2/rev in both hover and cruise. The first pitch/torsion mode is at 57 Hz (off scale). Frequency placement of the second flap/lag mode could be better at hover rpm to avoid 3/rev, but this design is intended to be only the starting point for design variations, so ideal frequency placement is not necessary at this time.

Airfoil Technology

To simulate advanced airfoils, airfoil coefficient tables were constructed based upon projected improvements beyond existing airfoil capabilities. These projections were based on CFD analysis and modern rotor airfoil trends. This approximates the results of a full airfoil design effort, parallel in concept to the technology projection utilized by RC. The "virtual airfoils" represented by these tables simulate performance levels expected of state-of-the-art, purpose-designed airfoils (see Refs. 16 and 17 for examples applicable to LCTR1). The LCTR2 Reference Airfoil (LRA) tables were constructed to be generally compatible with XN-series characteristics (Ref. 15), with slight performance improvements consistent with more modern airfoils.

Table 3 summarizes the airfoil performance targets and compares them to performance goals for the XN-series airfoils used on the JVX rotor. The airfoils are designated by their nominal *t/c* (e.g., LRA-09 is 9% thick). The coefficients at M = 0.0 are extrapolated from low airspeeds. The airfoil radial locations, in order of decreasing *t/c*, are 0.225, 0.50, 0.75, and 1.00 *R* (the same as the JVX test rotor, Ref. 12).

Wing Design and Modeling

The LCTR1 wing structural design was driven primarily by 2-g jump takeoff loads and by adequate stiffness to avoid whirl flutter. Table 4 summarizes the design requirements, which were the same for LCTR2. The structural properties (composite plies) were tapered from root to tip to minimize weight, which saved about 1100 lbs compared to a wing with constant properties (scaled LCTR1 weight saving based on RC sizing).

For LCTR2, the LCTR1 wing structure was first chord-scaled to LCTR2 dimensions. However, the jump take-off loads did not scale the same as wing chord, and the resulting structure was slightly understrength. Flapwise strength, hence stiffness, was accordingly increased. At this stage of the design evolution, aeroelastic stability proved inadequate, primarily due to coupling of the first rotor lag mode with wing torsion, so wing torsion stiffness was also increased.

Table 3. Airfoil performance comparison (Ref. 15).

Performance goal	XN09	LRA-09
$c_{l\max}$	1.35, $M = 0.6$	1.15, $M = 0.5$
c_d @ $c_l = 0.3$	0.006 @ $M = 0.75$	0.006 @ $M = 0.6$
c_m @ $M = 0.0$	−0.02	−0.026
M_{dd} @ $c_l = 0.3$	0.81	0.76
Hover $L/D_{\max}$	80 @ $M = 0.65$	90 @ $M = 0.55$
	XN12	LRA-12
$c_{l\max}$	1.40, $M = 0.45$	1.40, $M = 0.4$
c_d @ $c_l = 0.2$	0.006 @ $M = 0.65$	0.007 @ $M = 0.60$
c_m @ $M = 0.0$	−0.03	−0.02
M_{dd} @ $c_l = 0.2$	0.72	0.72
Hover $L/D_{\max}$	95 @ $M = 0.5$	90 @ $M = 0.4$
	XN18	LRA-18
$c_{l\max}$	1.5, $M = 0.3$	1.7, $M = 0.3$
c_d @ $c_l = 0.0$	0.007 @ $M = 0.57$	0.007 @ $M = 0.55$
c_m @ $M = 0.0$	−0.05	−0.05
M_{dd} @ $c_l = 0.0$	0.64	0.69
Hover $L/D_{\max}$	80 @ $M = 0.3$	90 @ $M = 0.3$
	XN28	LRA-28
$c_{l\max}$	1.35, $M = 0.19$	1.3, $M = 0.15$
c_d @ $c_l = 0.0$	0.018 @ $M = 0.51$	0.013 @ $M = 0.5$
c_m @ $M = 0.0$	−0.12	−0.08
M_{dd} @ $c_l = 0.0$	0.59	0.61
Hover $L/D_{\max}$	50 @ $M = 0.2$	80 @ $M = 0.2$

Table 4. Wing structural design requirements.

Purpose-designed wing airfoil (24% *t/c*),
constant chord & section (Ref. 16)
Spar placement from AFDD designs (Ref. 18)
Loads criteria (RC gross weight):
2-g jump takeoff loads
2-g symmetrical pullout with 75-deg pylons
2.5-g pullout with 0-deg pylons
2.0-g landing/taxi loads
Flutter margin 50% over cruise speed
IM7/8552 (graphite)
Tsai-Wu strength criteria, 1.5 factor of safety (Ref. 14)
Non-structural weight allowance for fuel tanks etc.
(RC tech factors)

Airframe Structural Model

The wing structural properties (inertia, stiffnesses, elastic axis, etc.) were incorporated into a finite element model of the airframe. Key parameters were then varied to analyze their effect on aeroelastic stability, as detailed in the section Stability Calculations. A simple elastic-line

model was used as the baseline, derived from models developed by AFDD (Ref. 18). It included non-structural wing masses, flexible nacelles with rotor masses, and a flexible fuselage. The model comprised ten elastic wing spar elements and two elastic elements for the fuselage and each nacelle (16 elastic elements total). The layout is shown in Fig. 4. A rigid, massless V-tail was included to help visualize the modes. The nacelle model is equivalent to the on-downstop configuration.

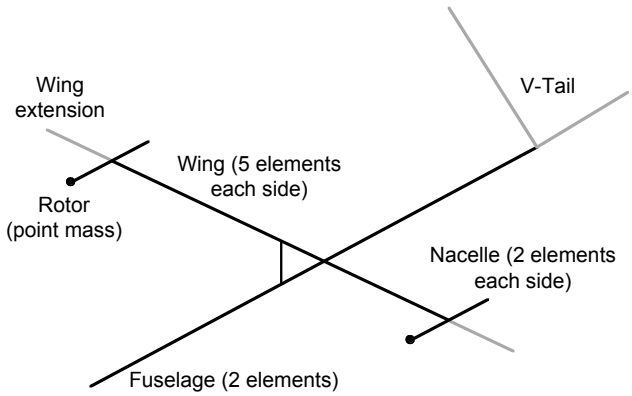

Fig. 4. Elastic-line finite element model of the LCTR2.

The finite element model was realized within CAMRAD II using its "core" modeling capability to compute mode shapes, frequencies, and modal masses for each variation of the airframe structure. CAMRAD II then coupled the airframe modes to rotor modes to get a complete flutter solution. The CAMRAD II architecture allowed the airframe modes to be pre-calculated and stored, with some savings in computational time. This was justified because rotor parameters do not directly affect the uncoupled airframe modes. The rotor modes were always recalculated for the final analyses, even if the rotor model was unchanged.

Certain simplifications were applied to the finite element model as appropriate for a conceptual design: there was no wing sweep, and the nacelle center of gravity was assumed to coincide with the wing elastic axis. The masses of the wing tip extensions are small compared to the nacelles and were therefore lumped into the nacelle masses. Fuselage, wing, and nacelle inertias were each scaled separately from the LCTR1 design, based upon the geometries sized by RC.

At this stage of the conceptual design process, the airframe structural dynamics model is necessarily very simple, but an elastic-line model is adequate to obtain the low frequency modes that are important for whirl flutter (Ref. 18).

The resulting baseline modal frequencies are given in Table 5. The modes are labeled according to their dominate, uncoupled mode shape. The first four wing frequencies lie within 0.3 Hz of each other, and all symmetric/ antisymmetric pairs are within 0.2 Hz. Furthermore, all of the modes are greater than 1/rev in cruise. The torsion modes are well separated from the bending modes only because the torsion stiffness was increased to avoid coupling with the rotor first lag mode. Designing the wing to per-rev frequency placement was inapplicable here.

Fuselage geometry effects the wing modes indirectly via inertial boundary conditions. The long, narrow LCTR2 fuselage (Fig. 1) has relatively high pitch and yaw inertia, which combines with the stiff wing center section to reduce modal deflections at the wing/fuselage junction. The resulting mode shapes and frequencies are very similar for each symmetric/antisymmetric mode pair.

Whirl Flutter Analysis

CAMRAD II couples the airframe modes (precalculated) to rotor aeroelastic modes (internal calculations) to get a complete flutter solution. To get a conservative whirl-flutter boundary, the CAMRAD II model assumes structural damping of 3% critical for both the rotor and wing in cruise, but no wing aerodynamic damping (Table 6). The high level of blade structural damping includes a large contribution from the pitch bearing; the value used is based on experience with hingeless rotors (Ref. 19). The flutter model includes ten elastic blade modes, so blade flutter is automatically included in the stability analysis. To speed convergence, only six blade modes were used in trim. The swashplate was effectively rigid, so its modes were at extremely high frequency and could be ignored.

Table 5. Modal frequencies for LCTR2 baseline wing.

Symmetric Modes				Antisymmetric Modes			
Frequency		Mode		Frequency		Mode	
Hz	Per rev			Hz	Per rev		
2.33	1.19	Wing chordwise bending,	SWC	2.31	1.18	Wing chordwise bending,	AWC
2.41	1.23	Wing beamwise bending,	SWB	2.60	1.33	Wing beamwise bending,	AWB
6.32	3.23	Wing torsion,	SWT	6.25	3.19	Wing torsion,	AWT
Cruise 1/rev = 1.96 Hz (117.53 rpm)							

The engine and drive-train technology is based on LCTR1 (Ref. 1) and scaled to LCTR2 size. The CAMRAD II aeroelastic model used a rigid drive train that included all rotating inertias but no shaft flexibility, as appropriate for the current level of analysis.

Table 6. CAMRAD II flutter model.

Cruise Stability
10 elastic modes per blade
6 wing/fuselage modes (Table 5)
rigid drive train (rotational inertia, but no shaft flexibility)
3% critical blade structural damping
3% critical wing structural damping
no wing aerodynamic damping
dynamic inflow, 3 axes
swashplate, 3 axes
symmetric/antisymmetric analysis, 96 modes total

Stability Calculations

For cruise stability calculations, the rotor was trimmed to two conditions known to simulate extremes of whirl flutter behavior: 1) the rotor trimmed to zero power; and 2) the rotor trimmed to thrust equal to aircraft drag up to the cruise speed for a given altitude, then trimmed to constant power at higher speeds (equivalent to a powered descent). Stability was calculated for the specified mission cruise conditions at 28,000 ft (Table 2) and at sea level. The target flutter boundaries were 450 knots at 28,000 ft (1.5 x 300 knots) and 375 knots at sea level (1.5 x 250 knots).

Baseline Stability

The critical condition for whirl flutter proved to be a constant-power descent at sea level. The target flutter speed was 375 knots (1.5 x 250 knots). The rotor first lag mode, coupled with the wing symmetric torsion mode (SWT), was just barely unstable at the target speed (Fig. 5). This is nearly ideal for aeroelastics studies, because it maximizes the sensitivity to parameter variations at zero damping. The symmetric modes were slightly less stable than the antisymmetric modes, but the trends are generally similar in that the lag mode was far more sensitive to airspeed than any other mode.

Only symmetric modes are shown in this paper, because they were nearly always the worst case modes, and because the trends for the most sensitive antisymmetric modes were always very similar to their symmetric counterparts. Frequency trends are not shown unless there is a large or highly nonlinear variation. All trends are plotted for 375 knots, constant-power descent at sea level (the worst case for the baseline model) unless otherwise specified.

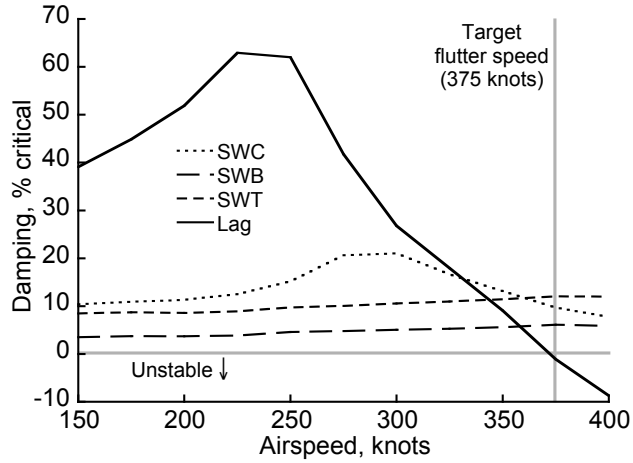

a) damping

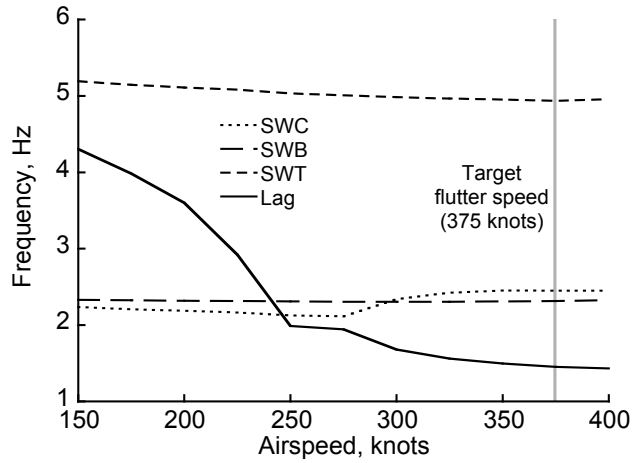

b) frequency

Fig. 5. Damping and frequency trends for symmetric modes, baseline model, sea level.

The most significant LCTR2 design change from Ref. 2 is the increased cruise tip speed of 400 ft/sec, which slightly improves cruise efficiency. The effect of tip speed on stability at 375 knots is shown in Fig. 6. Blade twist is reoptimized for every tip speed (Ref. 2). Reverting to the original tip speed of 350 ft/sec yields a significant improvement in stability (nearly 5%) as the lower dynamic pressure along the rotor blades reduces the perturbational forces that destabilize the wing/rotor system.

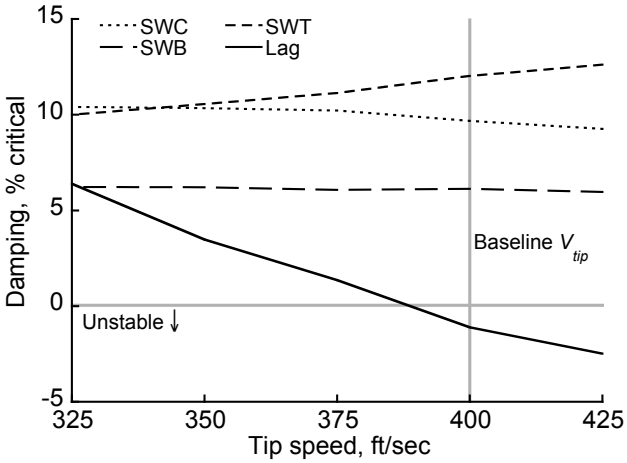

Fig. 6. Damping trends for tip speed variations, airspeed is 375 knots at sea level.

Solidity and Precone

Two top-level rotor design parameters—solidity and precone—were examined for their effects on whirl-mode stability. Figure 7 shows the effect of solidity variations. This is purely aerodynamic solidity; the effect of blade mass is discussed in the next section. Variations are biased towards higher values, because of the results of Ref. 2. Were it not for a mode interaction near $\sigma = 0.145$-0.150, the trend would be linear. The trend is significant and reflects the increasing perturbational forces as the blade chord gets larger.

The effects of precone are shown in Fig. 8. The trend is very strong and nearly linear for reasonable values of precone. The strong effect of precone is in keeping with past experience (Ref. 20). Re-analyzing precone with higher blade stiffness (not shown) confirmed that this is an effect of pitch-lag coupling.

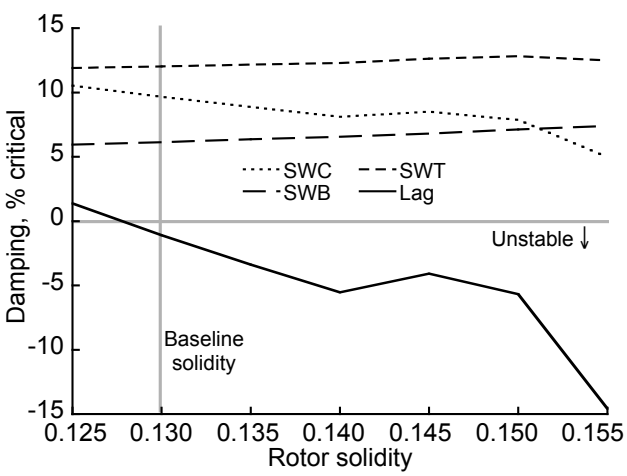

Fig. 7. Damping trends for rotor solidity variations, 375 knots at sea level.

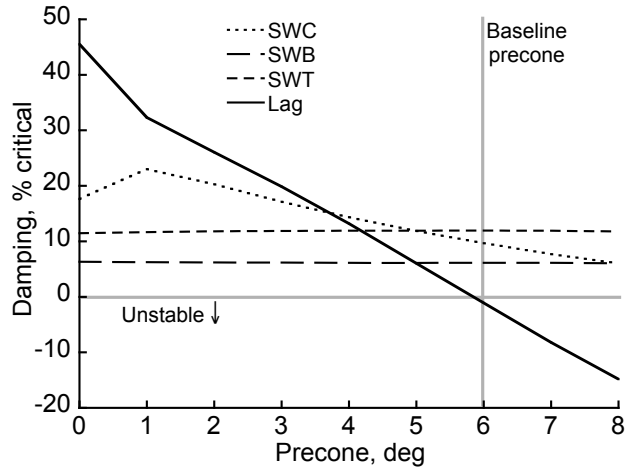

Fig. 8. Damping trends for rotor precone variations.

Mass Effects

The effects of mass variations on stability were separated into three categories: the distributed mass of the wing, the distributed mass of the rotor blades, and the effective point mass of the rotor at the hub. The first two allow comparison of the effects of wing structural mass to those of blade mass; these effects are manifest in the wing and rotor dynamics, respectively. The third is a simplified examination of the effects of nacelle inertia.

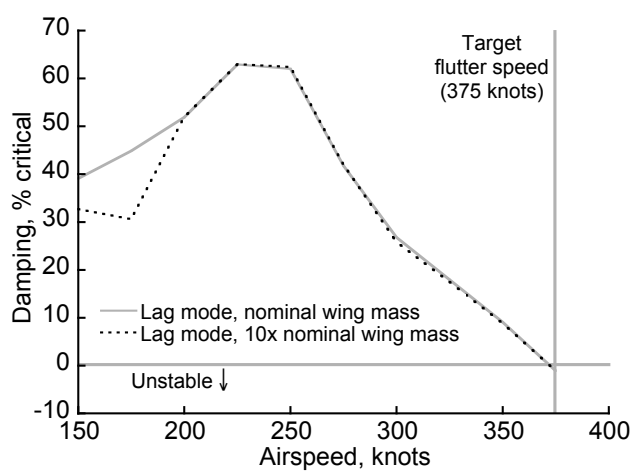

Fig. 9. Comparison of damping trends for nominal and 10x wing structural mass.

In RC, the wing structural mass (the torque box) is accounted for separately from non-structural mass (flaps, drive shaft, anti-icing, fuel system, etc.). This is reflected in the finite element model. The wing structural mass is 6505 lb, or 39% of the total wing mass (zero fuel). In Fig. 9, only the structural mass was changed. The trends are virtually indistinguishable at high speeds.

Figure 10 shows the damping and frequency trends as blade mass is varied from 0.1x to 10x the nominal value (337 lb per blade). While there is a large, nonlinear change in torsion frequency (SWT), the least stable mode (blade lag) varies slowly with blade mass until about 6x nominal, when there is a mode interaction with the flapwise bending mode (SWB).

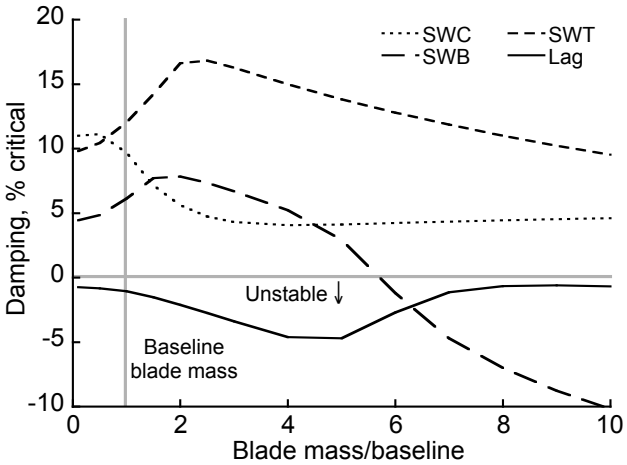

a) damping

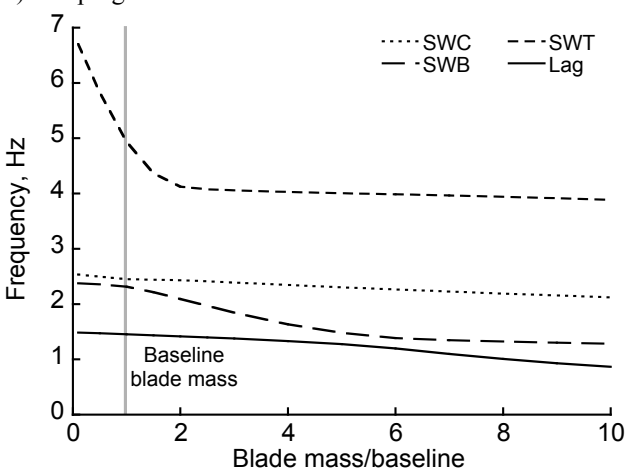

b) frequency

Fig. 10. Damping and frequency trends for 0.1x to 10x baseline rotor blade mass.

Nacelle mass and inertia variations present a dilemma: rotor mass; its distance from the wing elastic axis, nacelle center of gravity, and nacelle pivot; nacelle mass balance about the pivot (first mass moment); moment of inertia (second mass moment); total mass; and mass distribution are all intimately linked. No single parameter can be varied without changing at least one other. For this study, the expedient was taken to vary only the effective rotor mass, which in the airframe structural model is a point mass at the rotor hub (hence the label "hub mass" to distinguish it from individual blade mass). This value is the total rotor mass calculated by RC (4378 lb per rotor, Table 2). The total nacelle mass is 8567 per side. Because it is on the longest possible moment arm in the nacelle, the rotor mass has the largest possible effect on nacelle inertia, hence the wing modes.

Figure 11 shows the effect of hub mass variations (0.1x to 10x nominal) on total system damping. While the effect on the chord mode (SWC) is significant, the effect on the least stable mode—the lag mode— is very weak, even for very large variations.

Drive train inertia was varied from 0.1x to 10x nominal. The total change in damping of the lag mode was 1%—an insignificant amount compared to other variations shown herein, hence not plotted.

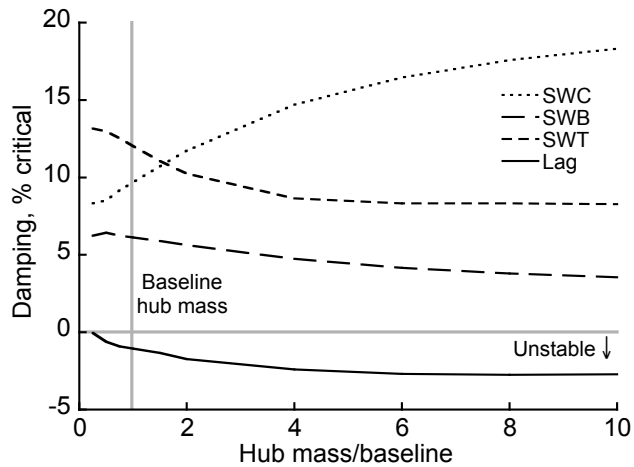

Fig. 11 Damping trends for 0.1x to 10x baseline rotor hub mass (point mass in airframe model).

Taken together, Figs. 9-11 indicate that mass variations do not have a major effect on whirl flutter. Not surprisingly, blade mass has the strongest effect, but even that is small compared to other parameters, as will be shown. Because of the relatively weak effect of structural masses on whirl flutter, stiffness and other parameters were freely varied without attempting to match structural mass to the structural stiffness. This can be expected to exaggerate the effect of most stiffness variations, but is acceptable given the weak sensitivity of damping to mass.

Wing Structural Properties

Wing elastic properties were separately varied for flapwise, chordwise, and torsional stiffness. For these three parameters, no attempt was made to design a practical wing structure—the goal was simply to determine the relative importance of those stiffness parameters. A more realistic analysis was to vary the amount of structural tapering of the wing from fully tapered to untapered. Again, no wing structure was actually designed: it was simply assumed that dropped plies and other property variations could be progressively reverted to the untapered configuration.

Figure 12 shows the damping and frequency trends for variations in wing flapwise stiffness. The trends are asymptotic at extremely high stiffness. Note the frequency crossing and consequent modal interaction near nominal stiffness, and the mode interaction near 3x nominal stiffness. The modal couplings are unfavorable, such that higher stiffness reduces lag-mode stability, even though flapwise bending-mode stability (SWB) is much improved.

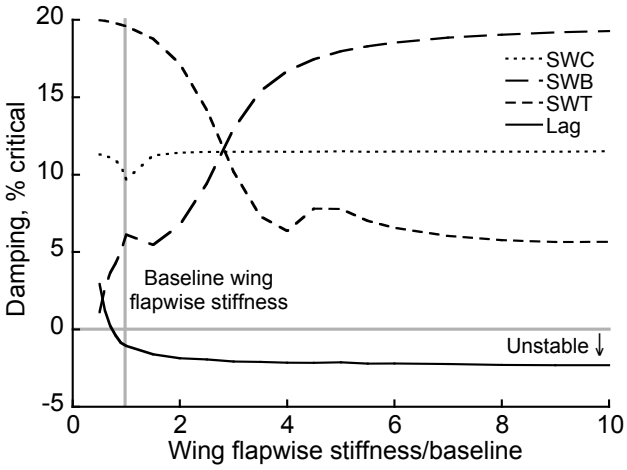

a) damping

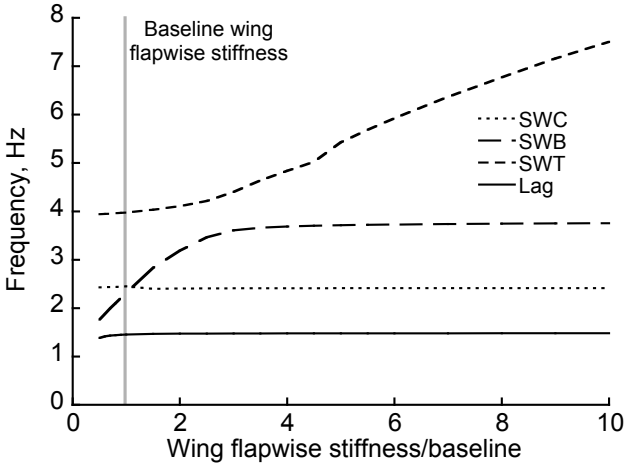

b) frequency

Fig. 12. Damping and frequency trends for wing flapwise stiffness.

Figure 13 shows the trends for variations in wing chordwise stiffness. There is a strong interaction near the nominal stiffness and a second, weaker interaction near 5x nominal stiffness. Compared to Fig. 12, the couplings are more favorable: higher chordwise stiffness improves lag-mode stability, but a reduction in SWB damping limits the total effectiveness. The optimum value is about 1.5x nominal stiffness.

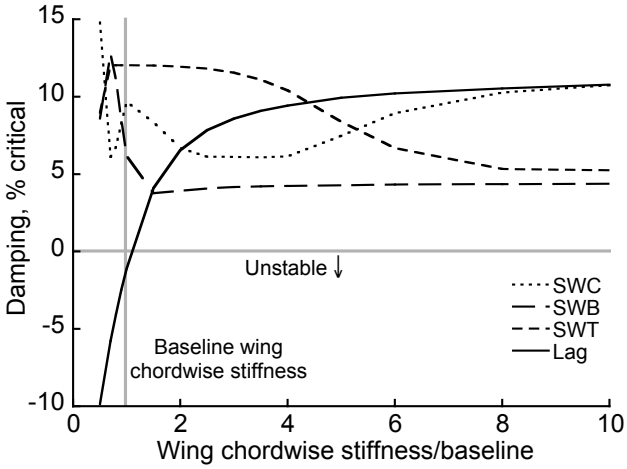

a) damping

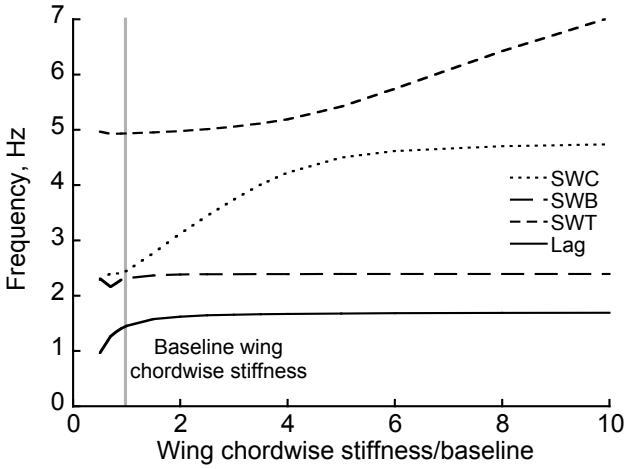

b) frequency

Fig. 13. Damping and frequency trends for wing chordwise stiffness.

Figure 14 shows the trends for variations in wing torsional stiffness. The highly nonlinear behavior is again evident. Damping always improves with increased stiffness, although the effect is asymptotic from about 2x nominal stiffness and never reaches the maximum level provided by increased chordwise stiffness (Fig. 13).

Figure 15 shows the effect of varying the amount of structural taper. Damping is plotted against tip/root ratio for flapwise (perpendicular to chord) stiffness, which had the most taper for any wing structural parameter (flapwise, chordwise, and torsional stiffness tip/root ratios were all less than 0.14, as was mass). The results suggest that the wing structure was more highly tapered than optimum for stability. Lag damping could be improved by almost 6% for a slight weight penalty of 40% of the expected savings from tapering the structure. Although it is little affected by taper, the bending mode (SWB) nevertheless limits the effectiveness of reducing taper. The frequency variations are much smaller and more linear than those of Figs. 12-14 and are not shown.

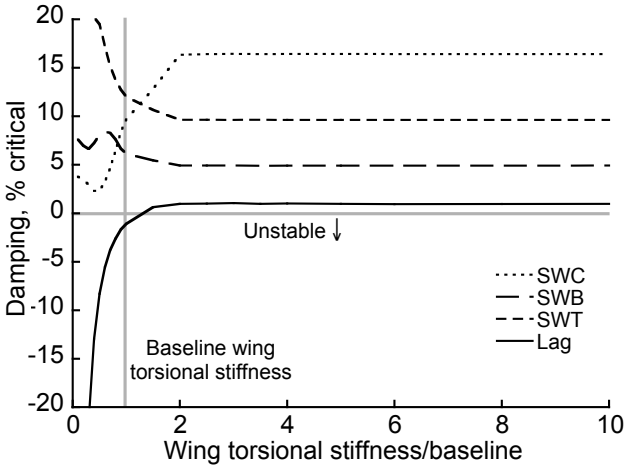

a) damping

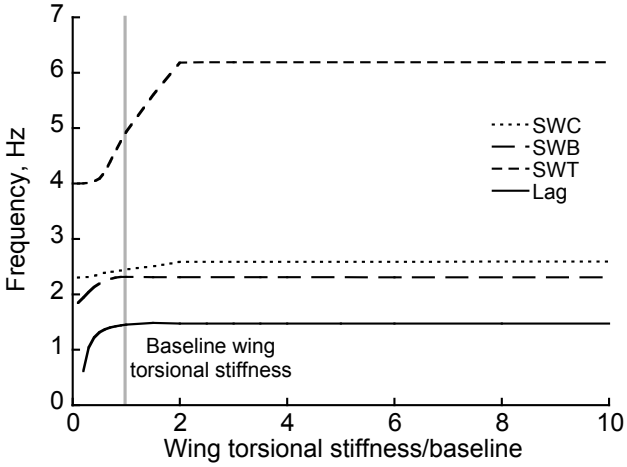

b) frequency

Fig. 14. Damping and frequency trends for wing torsional stiffness.

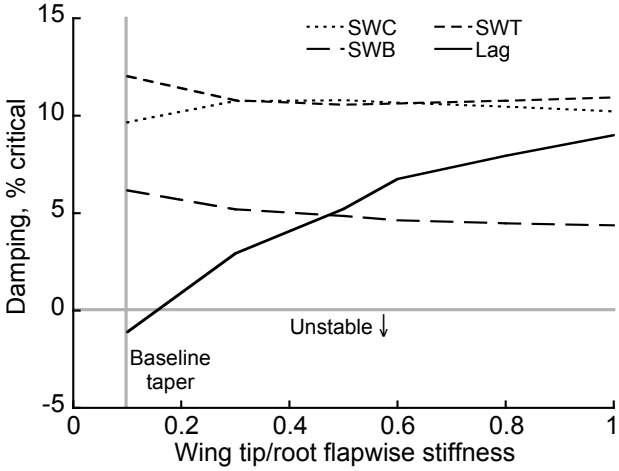

Fig. 15. Damping trends for wing structural taper variations.

Rotor Structural Properties

Several rotor structural properties were varied to allow comparison of the relative sensitivity of whirl mode stability to rotor versus wing properties. These include control-system stiffness, and blade flap, lag and torsional stiffness. Blade mass effects were covered in the Mass Effects subsection, above.

Control-system stiffness is here lumped into pitch-link stiffness (swashplate stiffness is extremely high). The nominal model had an effectively rigid control system. Figure 16 shows the effect of varying pitch-link stiffness. Multiple mode interactions distort the curve of the least stable mode. An additional curve is added with two times nominal blade torsional stiffness (GJ), which avoids the interactions and better reveals the underlying nonlinearity of pitch-link stiffness. The curve is shifted up enough to fully stabilize the system at about $5*10^6$ lb/ft stiffness. The largest variations in frequency were seen in the lag and wing torsion modes, but were less than ±0.02 Hz, so no frequency curves are shown.

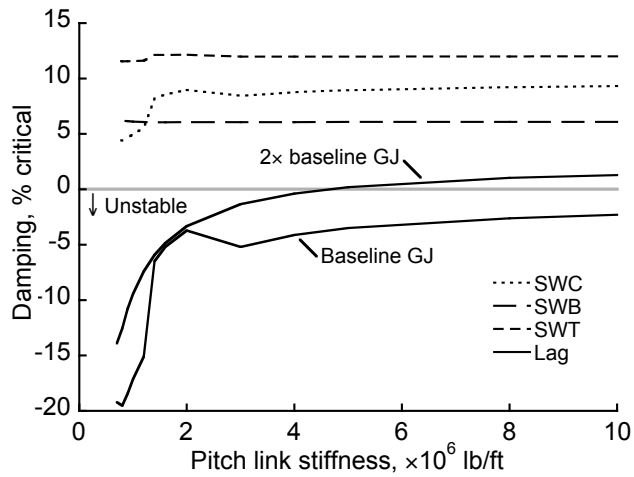

Fig. 16. Damping trends for pitch-link stiffness variations.

Figure 17 shows the effects of varying blade flapping (flapwise) stiffness, plotted as a ratio with respect to the nominal stiffness. Stiffness is multiplied by a uniform ratio along the entire radius. Blade flapping stiffness is by far the most sensitive parameter examined. A 20% increase in stiffness was enough to make wing bending (SWB) the critical mode. The high sensitivity of damping to flapping stiffness is not surprising for a hingeless rotor, although the nearly linear behavior below three times nominal stiffness was unexpected, especially for such large changes in damping.

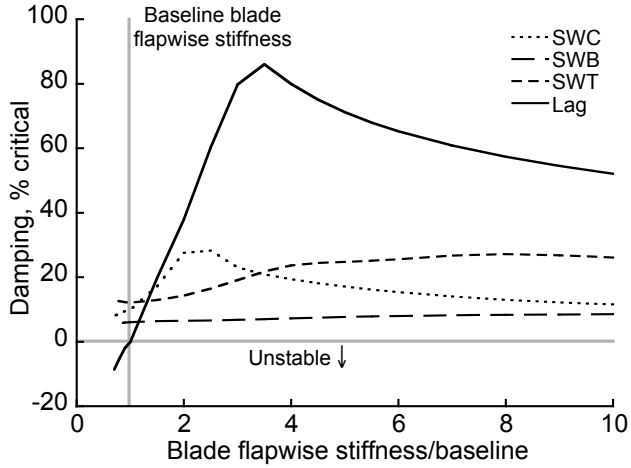

a) damping

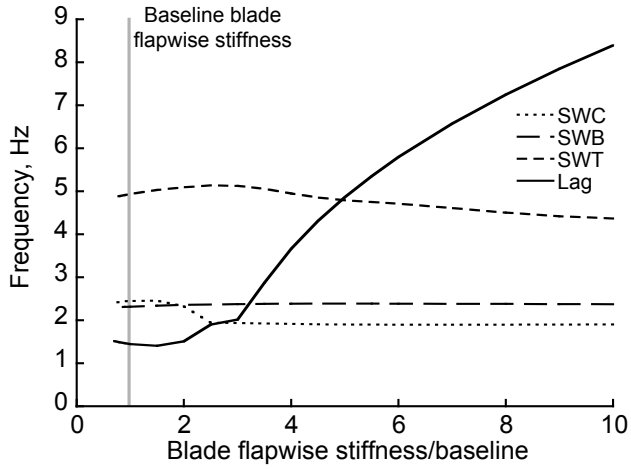

b)frequency

Fig. 17. Damping and frequency trends for blade flapping (flapwise) stiffness variations.

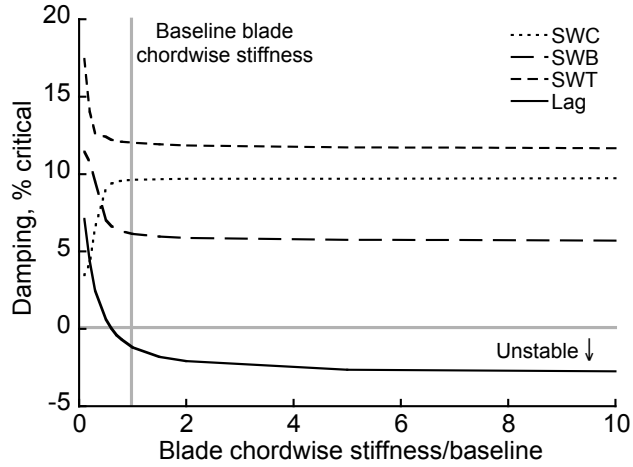

a) damping

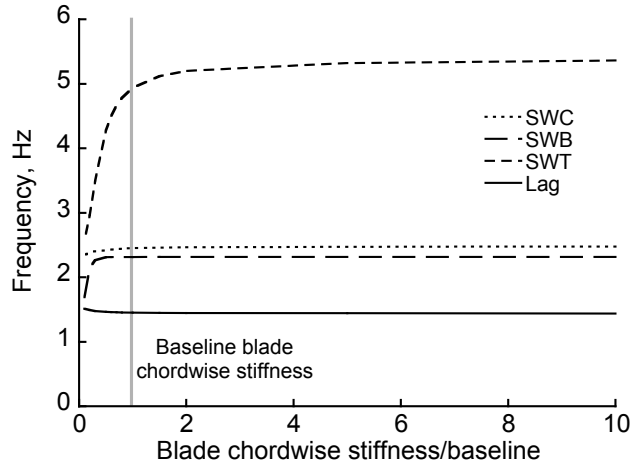

b) frequency

Fig. 18. Damping and frequency trends for blade lag (chordwise) stiffness variations.

Figure 18 shows the effects of varying blade lag (chordwise) stiffness, ratioed to nominal stiffness. The effects are strongly nonlinear, with high stiffness leading to lower damping, although this effect quickly approaches an asymptotic limit of about −2.7% (compared to −1.2% nominal). At very low stiffness, the chord mode becomes the least stable mode. While the lag mode has the greatest variation in damping, it has the least variation in frequency.

Figure 19 shows the effects of varying blade torsional stiffness. Yet again, there is a strongly nonlinear variation in the least stable mode, with little variation in frequency (less than ±0.014 Hz, hence not shown). The wing chord mode follows a similar nonlinear trend to the lag mode, but with reduced sensitivity.

Taken together, these results imply that the rotor could be slightly softer in-plane, but stiffer out-of-plane and in torsion. However, loads have not been taken into account, nor have practical issues of manufacturability. Furthermore, these results are for a hingeless rotor, in which the entire structure rotates with the pitch bearing. A flexured rotor, with the flexure isolated from pitch changes (similar to the V-22, but without the gimbal), would be expected to behave differently, as would a fully gimballed rotor. Nevertheless, these results indicate the appropriate directions in which to pursue aeroelastically tailored rotors.

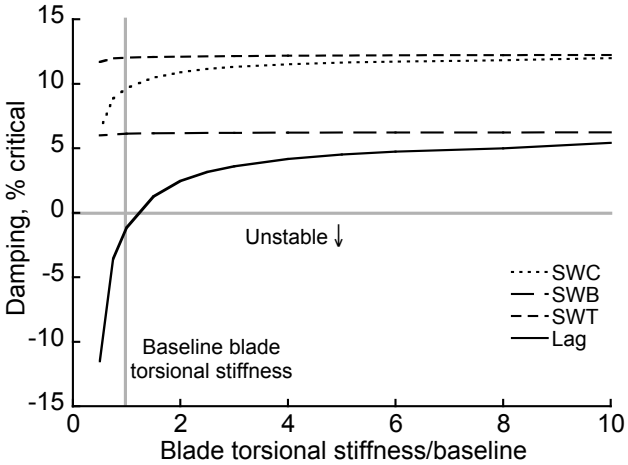

Fig. 19. Damping trends for blade torsional stiffness variations.

Common Trends

Several variations of both wing and rotor properties had similar trends of damping versus stiffness ratio. Wing flapwise, chordwise, and torsional stiffness (Figs. 12-14), and rotor pitch-link, lag, and torsional stiffness (Figs. 16, 18 and 19) all followed nearly the same nonlinear trend; the trends for wing flapwise stiffness and rotor lag stiffness were inverted (Figs. 12 and 18). These trends asymptotically approached the maximum damping (or worst-case negative damping, in the case of the inverted trends) above about twice the baseline stiffness values. Below about one-half the baseline values, the trends become severely negative; in the two inverted cases, a different mode became unstable. (No baseline value was defined for pitch-link stiffness, but the nonlinearity was the same, more clearly in the case of doubled blade torsional stiffness.) This suggests that there is a narrow, nonlinear range between minimum acceptable stiffness and optimum stiffness (minimum weight).

While it would be gratifying to believe that this proves that the baseline wing design was optimal, it is perhaps more likely that the common nonlinearity reflects strong modal coupling between the hingeless rotor and the wing. A small increase in nearly any stiffness parameter is enough to decouple the modes (or in the case of wing flapwise stiffness and rotor lag stiffness, a decrease in stiffness). A change in the reverse sense leads to stronger modal coupling and a precipitate drop in damping.

The common nonlinearity frustrates any attempt to incorporate a simple aeroelastic stability criterion into a design code. If the nonlinear effect can be shown to be unique to this combination of baseline wing and rotor parameters, then there is hope that a different baseline (such as a flexured rotor or structurally untapered wing) may yield more tractable results. On the other hand, if this effect is typical of large, slowed proprotors combined with wings of similar scale, then such nonlinearities will make design optimization for stability inherently difficult.

Conclusions

Aeroelastic stability in cruise (whirl flutter) was examined for the NASA Large Civil Tiltrotor (LCTR2). The effects on stability of wing and rotor structural properties (mass and stiffness), control-system stiffness, solidity, precone, and cruise tip speed were examined using CAMRAD II. The critical requirement is adequate whirl-flutter speed margin in cruise, with the worst case (minimum stability) at constant power at sea level. The first rotor lag mode, coupled with the wing torsion motion, was the critical mode for stability.

Structural mass of both the wing and rotor had little effect on stability. Precone, tip speed, and solidity affected stability as expected: reducing any of these parameters improved damping of the critical modes.

Rotor flapwise stiffness was by far the most sensitive parameter examined, with a nearly linear effect on lag-mode damping up to about three times nominal stiffness. Several other parameters—wing flapwise, chordwise, and torsional stiffness, and rotor pitch-link, lag, and torsional stiffness—all had strongly nonlinear effects on stability, with common nonlinearities in the damping trends. These nonlinearities imply that although the LCTR2 wing design was close to optimum, the optimum wing design may be very sensitive to the rotor baseline design.

Recommendations

Recommendations for further exploration of aeroelastic stability of very large tiltrotors can be grouped into three areas: updating the LCTR2 concept, examination of alternative rotor concepts, and incorporation of more advanced technologies.

The results of the present study should be combined with those of Ref. 11 to define a revised LCTR2, in order to establish a more rigorous baseline against which to compare more detailed design tradeoffs. For example, lowering tip speed would improve whirl flutter stability, with a possible wing weight saving, but would slightly degrade cruise efficiency, with a consequent cost in fuel weight. Determination of the optimum balance requires application of a sizing code such as RC, and as such is beyond the scope of this paper. In light of the strongly nonlinear effects of wing and rotor stiffness, the wing and rotor structural designs should also be closely re-examined to ensure the baseline designs are appropriate.

With an updated baseline in hand, different rotor configurations should be examined, including a flexured rotor (either coning or flapping flexure); a gimballed rotor, with and without delta-3 limits; and a rotor with conventional, higher tip speed (single-speed gearbox).

Parallel investigations should include an untapered (or partially tapered) wing structure. An important objective of these investigations is to determine whether any alternative concepts are subject to the highly nonlinear sensitivity of stability (damping) to structural stiffness seen for the baseline LCTR2 design.

A variety of advanced technologies have been studied for tiltrotors, but not always for very large vehicles like LCTR2, or for slowed rotors. At a minimum, the research should be extended to include aeroelastically tailored structures for the wing and rotor, and active and passive stability augmentation. The different ratios of rotor speed to wing frequencies for very large tiltrotors may change the relative benefits of such technologies compared to previous results.

The aeroelastic stability calculations performed in this investigation are typical of the analyses that must be conducted as part of the process of rotorcraft conceptual and preliminary design. A goal of this research is to develop the aeroelastic analysis interface and environment further in order to improve the effectiveness and efficiency of the design process. Conducting extensive parametric variations in order to develop empirical scaling rules for the conceptual design codes is still a goal. In the long term however, the desired approach is to be able to quickly assess the aeroelastic characteristics of advanced designs and provide information regarding design parameters to the sizing codes. Exploring this type of integrated design and analysis is an aspect of planned future work.

Acknowledgments

The authors wish to thank Gerardo Nuñez of the U. S. Army Aeroflightdynamics Directorate (AFDD) for his assistance in the layout of the LCTR2, and Dr. Michael P. Scully, also of AFDD, for his critique and guidance on the aircraft design process and appropriate technology assumptions.

References

1. Johnson, W., Yamauchi, G. K., and Watts, M. E., "NASA Heavy Lift Rotorcraft Systems Investigation," NASA TP-2005-213467, September 2005.

2. Acree, C. W., Yeo, H., and Sinsay, J. D., "Performance Optimization of the NASA Large Civil Tiltrotor," International Powered Lift Conference, London, UK, July 2008; also NASA TM-2008-215359, June 2008.

3. Sinsay, J. D., "The Path to Turboprop Competitive Rotorcraft: Aerodynamic Challenges," AHS Specialists' Conference on Aeromechanics, San Francisco, California, January 2008.

4. Acree, C. W., and Johnson, W., "Performance, Loads and Stability of Heavy Lift Tiltrotors," AHS Vertical Lift Aircraft Design Conference, San Francisco, California, January 2006.

5. Johnson, W., "CAMRAD II Comprehensive Analytical Model of Rotorcraft Aerodynamics and Dynamics," Johnson Aeronautics, Palo Alto, California, 2005.

6. Deckert, W. H. and Ferry, R. G., "Limited Flight Evaluation of the XV-3 Aircraft," Air Force Flight Test Center Report AFFTC-TR-60-4, May 1960.

7. Karem, A., "Optimum Speed Tilt Rotor," United States Patent 6,641,365 B2, Nov. 4, 2003.

10. Preston, J., and Peyran, R., "Linking a Solid-Modeling Capability with a Conceptual Rotorcraft Sizing Code," AHS Vertical Lift Aircraft Design Conference, San Francisco, California, January 2000.

11. Yeo, H., Sinsay, J. D., and Acree, C. W., "Blade Loading Criteria for Heavy Lift Tiltrotor Design," AHS Southwest Region Technical Specialists' Meeting, Dallas, Texas, October 2008.

12. Acree, C. W., "Calculation of JVX Proprotor Performance and Comparisons with Hover and High-Speed Test Data," AHS Specialist's Conference on Aeromechanics, San Francisco, California, January 2008.

13. Acree, C. W., "Modeling Requirements for Analysis and Optimization of JVX Proprotor Performance," AHS 64th Annual Forum, Montréal, Canada, April 2008.

14. Zhang, J., and Smith, E., "Design Methodology and Cost Analysis of Composite Blades for a Low Weight Rotor," AHS Vertical Lift Aircraft Design Conference, San Francisco, California, January 2006.

15. Narramore, J. C., "Airfoil Design, Test, and Evaluation for the V-22 Tilt Rotor Vehicle," AHS 43rd Annual Forum, St. Louis, Missouri, May 1987.

16. Acree, C. W., Martin, P. B., and Romander, E. A., "Impact of Airfoils on Aerodynamic Optimization of Heavy Lift Rotorcraft," American Helicopter Society Vertical Lift Aircraft Design Conference, San Francisco, California, January 2006.

17. Martin, P. B., Rhee, M., Maughmer, M. D., and Somers, D. M., "Airfoil Design and Testing for High-Lift Rotorcraft Applications," AHS Specialist's Conference on Aeromechanics, San Francisco, California, January 2008.

18. Peyran, R., and Rand, O., "The Effect of Design Requirements on Conceptual Tiltrotor Wing Weight," AHS 55th Annual Forum, Montréal, Quebec, Canada, May 1999.

19. Kloppel, V., Kampa, K., and Isselhorst, B., "Aeromechanical Aspects in the Design of Hingeless/Bearingless Rotor Systems," Ninth European Rotorcraft Forum, Stresa, Italy, September 1983.

20. Johnson, W., "Analytical Modeling Requirements for Tilting Proprotor Aircraft Dynamics," NASA TN D-8013, July 1975.